HHS Public Access

Author manuscript

Phys Med Biol. Author manuscript; available in PMC 2018 May 10.

Published in final edited form as:

Phys Med Biol. 2016 August 21; 61(16): 6121–6131. doi:10.1088/0031-9155/61/16/6121.

A longitudinal magnetic resonance elastography study of murine brain tumors following radiation therapy

Y. Feng[1,2,3], **E. H. Clayton**[4], **R. J. Okamoto**[4], **J. Engelbach**[5], **P. V. Bayly**[4,6,7], and **J. R. Garbow**[5,8]

[1]School of Mechanical and Electronic Engineering, Soochow University, Suzhou, Jiangsu, China

[2]Robotics and Microsystems Center, Soochow University, Suzhou, Jiangsu, China

[3]School of Computer Science and Engineering, Soochow University, Suzhou, Jiangsu, China

[4]Department of Mechanical Engineering and Materials Science, Washington University, St. Louis, MO, USA

[5]Department of Radiology, Washington University, St. Louis, MO, USA

[6]Department of Neurological Surgery, Washington University, St. Louis, MO, USA

[7]Department of Biomedical Engineering, Washington University, St. Louis, MO, USA

[8]Alvin J. Siteman Cancer Center, Washington University, St. Louis, MO, USA

Abstract

An accurate and noninvasive *method for assessing* treatment response *following* radiotherapy is needed for both treatment monitoring and planning. *Measurement of solid tumor volume alone is not sufficient for reliable early detection of therapeutic response, since changes in physiological and/or biomechanical properties can precede tumor volume change following therapy*. In this study, we use magnetic resonance elastography (MRE) to evaluate the treatment effect after radiotherapy in a murine brain tumor model. Shear modulus was calculated and compared between the delineated tumor region of interest (ROI) and its contralateral, mirrored counterpart. We also compared the shear modulus from both the irradiated and non-irradiated tumor and mirror ROIs longitudinally, sampling *four* time points spanning 9 to 19 days post tumor implant. Results showed that the tumor ROI had a lower shear modulus than that of the mirror ROI, independent of radiation. The shear modulus of the tumor ROI decreased over time for both the treated and untreated groups. By contrast, the shear modulus of the mirror ROI appeared to be relatively constant for the treated group, while an increasing trend was observed for the untreated group. The results provide insights into the tumor properties after radiation treatment and demonstrate the potential of using *the* mechanical *properties* of the tumor as a biomarker. In future studies, more closely spaced time points will be employed for detailed analysis of the radiation effect.

Correspondence: Joel R Garbow, Ph.D., Campus Box 8227, 4525 Scott Avenue, St. Louis, MO 63110, garbow@wustl.edu.

1 Introduction

Accurate, non-invasive characterization of solid tumors during and following radiation treatment is important for monitoring therapeutic response and guiding subsequent treatment planning (Lupo and Nelson, 2014; Minamimoto *et al.*, 2015; Schmainda, 2012). Response is often monitored by measuring changes in tumor volume, using magnetic resonance imaging (MRI) or *X-ray computed* tomography (CT), weeks to months following radiation treatment. However, tumor volume change alone is a poor marker of positive therapeutic response, as important physiological and microstructural changes indicative of response may significantly precede tumor shrinkage. Thus, the development of non-invasive imaging techniques that can serve as biomarkers of early therapeutic response would be extremely valuable.

Positron emission tomography (PET) (Basu and Alavi, 2009; Suchorska *et al.*, 2014; Uslu *et al.*, 2015) and MRI (Jost *et al.*, 2007; Ellingson *et al.*, 2015) have been widely used to characterize brain tumors. PET can provide important metabolic information about tumors, and PET experiments employing a variety of tracers, including [^{18}F]fluorodeoxyglucose (FDG), [^{18}F]fluoroethyltyrosine (FET), and [^{18}F]fluoro-L-dopa (FDOPA), have been used to characterize response to radiotherapy (Bolcaen *et al.*, 2015; Juhasz *et al.*, 2014; Dunet *et al.*, 2015), though PET's low spatial resolution limits its ability to assess heterogeneity of response. MRI is used extensively to characterize tumors, due to its high soft-tissue contrast and superior image resolution. Beyond T1- and T2-weighted measurements of changes in tumor volume (Jost *et al.*, 2007; Leung *et al.*, 2014; Ellingson *et al.*, 2015), a number of different MR-based methods have been examined for evaluating treatment response, including diffusion imaging (Farjam *et al.*, 2014; Moffat *et al.*, 2006; Tsien *et al.*, 2014), perfusion imaging (Hakyemez *et al.*, 2005; Law *et al.*, 2008), and MR spectroscopy (Horska and Barker, 2010; Kumar *et al.*, 2015). Although these techniques have shown promise for detecting and characterizing recurrent tumors after radiation treatment, none represent current standard of care for assessing treatment response.

Magnetic resonance elastography (MRE) can provide important insights into tissue mechanical properties by imaging the propagation of acoustic waves within the tissue (Atay *et al.*, 2008; Clayton *et al.*, 2012; Sinkus, 2014; Johnson *et al.*, 2013; John *et al.*, 2012; Muthupillai *et al.*, 1995; Sack *et al.*, 2004; Sinkus *et al.*, 2000; Hatt *et al.*, 2015). MRE can detect differences in tumor stiffness relative to surrounding tissue (Reiss-Zimmermann et al., 2014; Simon et al., 2013; Xu et al., 2007; Krouskop et al., 1998; McKnight et al., 2002; Sinkus et al., 2005; Barton et al., 1999; Venkatesh et al., 2008) and has been applied clinically to diagnose liver fibrosis (Yin *et al.*, 2007; Huwart *et al.*, 2006; Wang *et al.*, 2011). Recent pilot studies in brain tumors found that meningiomas could be identified clearly by MRE, with the tumors having a complex-valued shear modulus that reflects increased stiffness (i.e., increased shear modulus) (Murphy et al., 2013), or increased viscosity (Reiss-Zimmermann et al., 2014) compared to healthy brain tissue. In this study, we investigated the potential of using shear modulus, measured by MRE, as a biomarker for characterizing tumor and evaluating response to radiation treatment. The shear moduli of irradiated brain tumors and contralateral reference regions were measured and compared at different time

points following radiation treatment, and also compared with the moduli of untreated tumors.

2 Materials and Methods

2.1 Animal preparation

Delayed brain tumor (DBT) glioblastoma cells were implanted into twenty female Balb/c mice, age 7–8 weeks, using previously published methods (Jost *et al.*, 2007). *All experiments were approved by the Animal Studies Committee at Washington University*. Mice were randomly separated into two groups, designated as A and B (n=10, each), and tumor implantation was staggered between the groups by one week. Mice were labeled M01A to M10A and M01B to M10B, respectively, and the day of tumor-cell implantation was designated as post-implantation day 0 (POD0). Initial, T2-weighted anatomical MR images were collected on POD8. Based on these images (Figure 1), twelve mice showing clear tumor growth were selected. Of these twelve, six mice were treated on POD10 with a single-fraction, 20-Gy dose of radiation, a dose previously demonstrated to slow DBT tumor growth, delivered to the tumor-bearing hemisphere using the Leksell Gamma Knife Perfexion (Elekta; Stockholm, Sweden), and six were untreated.

2.2 MRE

MRE experiments on mouse brain were performed on POD9, POD13, POD16, and POD19 using a dedicated, 4.7 T small-animal MR imaging system (Oxford magnet/Agilent DirectDrive1™ console). An actively decoupled transmit/receive coil pair (Garbow *et al.*, 2008) was used for acquiring the signal. Mice were anesthetized with isoflurane in O_2 (1.5% v/v) and body temperature was maintained at 37.0 +/- 1.0 °C using circulating warm water.

Mechanical waves at 1800 Hz were induced in the mouse brain using a tooth bar driven by a piezoelectric actuator, as described previously (Clayton *et al.*, 2011b). Motion-encoded phase images for each 3D motion component were acquired in the brain at four different phase points during one wave period. At each temporal point, 29 image slices of the brain were acquired with an imaging field of view (FOV) of 16 mm × 16 mm and an isotropic voxel size of $(0.25\ \text{mm})^3$. Phase image data were phase-unwrapped and smoothed with a 3 × 3 × 3 Gaussian filter (standard deviation, 1 voxel). To eliminate the effect of *displacement from* longitudinal wave ($\boldsymbol{u}_L$) and preserve only the *displacement component of* shear wave ($\boldsymbol{u}_T$), a curl operator was applied to the displacement field. Three adjacent slices were used for the 3D inversion. The complex shear modulus G^* is defined as $G^* = G' + iG''$, where G' and G'' are the storage and loss modulus, respectively. The value of G^* at each voxel was estimated by a total least square (TLS) fit (fitting window size, 5 × 5 × 3 voxels) to the wave equation (Feng *et al.*, 2013b; Okamoto *et al.*, 2011):

$$-\rho\omega^2\left(U'_{n0} + iU''_{n0}\right) = \left(G' + iG''\right)\left(\nabla^2 U'_{n0} + \nabla^2 U''_{n0}\right), \quad (1)$$

in which ω is the actuation frequency and $U_{n0} = U'_{n0} + iU''_{n0}$ is the complex valued fundamental Fourier component of the shear-wave displacement vector, $\boldsymbol{u}_T$, in all three *Cartesian* directions ($\boldsymbol{u}_T(\boldsymbol{r}, t) = \mathbf{U}_0(\boldsymbol{r})e^{i\omega t}$, where $\boldsymbol{r} = x_n\boldsymbol{e}_n$, $n = 1, 2, 3$). The TLS weighting parameter λ_{TLS} was set to 10, and a normalized residual error (NRE) was used to evaluate each estimate (Feng *et al.*, 2013a; Clayton *et al.*, 2011b; Okamoto *et al.*, 2011). Shear modulus estimates at a given voxel were rejected if NRE was larger than 0.8.

3 Results

Results for treated animals are shown for POD09, POD13, POD16, and POD19. Consistent with our previous results (Jost *et al.*, 2007), no untreated animals survived to POD16, hence MRE results for untreated animals are shown only for POD09 and POD13.

Parametric maps of the fundamental harmonic of the z-displacement (through-plane displacement) component, and estimated values of G′ and G″ for a representative mouse brain (M10A), are shown in Figure 2. The tumor/mirror ROI pair was manually contoured by masking the tumor ROI and its contralateral, mirrored ROI (no implanted tumor) with respect to the centerline of the brain (Figure 3a).

G′ and G″ values were both analyzed. However, G″ values showed relatively little difference between tumor and mirror ROI's across all PODs (Table 1). As a consequence, we focused this short communication on the analysis of G′. A histogram of the tumor/mirror ROI pair showed that the shear modulus, G′, of the tumor ROI is lower than its contralateral, mirrored ROI (Figure 3b, c). To demonstrate statistical differences in G′ values between the tumor and mirror ROIs, G′ was analyzed on a voxel-by-voxel basis for the *manually* contoured ROIs. G′ values, averaged across the ROIs, were calculated for each mouse, and the mean G′ value across each group was then computed. G′ values at each POD for both treated and untreated animals are summarized in Figure 4.

To measure the effects of radiation treatment, G′ values for each mouse at POD09 and POD13 were compared for the treated (Figure 4a, b) and untreated (Figure 4c, d) groups. To assess the significance of radiation treatment, we performed a two-way analysis of variance (ANOVA) of G′ values between the treated and untreated tumors, across all POD's. A similar ANOVA was performed for mirror ROI's in the treated and untreated groups. For the ANOVA analysis, the six mice from the treated and untreated groups provided six replicates each. For the tumor ROI group, p-values comparing G′ values for the treated/untreated, POD09/POD13, and the interaction between the two were 0.6993, 0.0290, and 0.8266, respectively. For the mirror ROI group, p-values comparing G′ values for the treated/untreated, POD09/POD13, and the interaction between the two were 0.2810, 0.0334, and 0.0823, respectively. For both the tumor and mirror ROIs, no meaningful differences were found between the treated and untreated groups, and POD was a more significant factor than treatment. To test the significance of the variation of G′ over time, separate, repeated-measures, one-way ANOVA tests were performed for the treated tumor ROI's and mirror ROI's (from the same treated mice). The six mice from the treated group provided six observations at each POD. P-values comparing the G′ value at different PODs were 0.2792 and 0.2174, respectively. Since no significant difference was observed in the above ANOVA

tests, post-hoc tests were not performed. In the POD09 mice, the largest absolute difference in G′ values between the treated and untreated tumor ROI's was 2.04 kPa, while in the POD13 group, it was 2.93 kPa.

For the treated group, the mean G′ value of the tumor ROI was lower than the contralateral, mirrored ROI for each mouse at each POD (Figure 4e). A paired student t-test showed the differences in mean G′ values between the tumor and mirror tissue regions at POD13, POD16, and POD19, respectively, were statistically significant ($p<0.05$). In the untreated group, the mean G′ value was also lower in the tumor ROI than in the contralateral mirrored ROI at both POD09 and POD13. The difference was statistically significant at both time points (Figure 4f).

For all mice in the radiation-treated group, the values of G′ in the tumor regions decreased as a function of post-implantation day, POD (Figure 4e). In the untreated tumor, the mean G′ values of the tumor ROIs also decreased for 5 of 6 mice. For each mouse, the time dependence of G′ vs. POD over all four PODs was fit with a linear function, the slope of the fitted line was calculated, and these slopes were averaged across all mice within a group. The mean slope of G′ vs. POD for the tumor regions (-0.457 kPa/day) was 3.4 times that of the mirror tissue region (-0.136 kPa/day), a statistically significant difference ($p<0.05$).

4 Discussion

Several groups have recently characterized tumors using MRE (Reiss-Zimmermann *et al.*, 2014; Simon *et al.*, 2013; Murphy *et al.*, 2013; Sahebjavaher *et al.*, 2015; Pepin *et al.*, 2014; Li *et al.*, 2014). A comprehensive *MRE* study of different types of human brain tumor, including glioblastoma, anaplastic astrocytoma, meningioma, and cerebral metastasis, showed different mechanical properties among these tumors (Reiss-Zimmermann *et al.*, 2014). In several of these studies, the tumors were found to be softer, i.e., to have a lower shear modulus, than healthy reference tissue (Simon *et al.*, 2013; Reiss-Zimmermann *et al.*, 2014). A recent human MRE study found that, with one exception, glioblastoma tissue is softer than healthy brain tissue (Simon *et al.*, 2013). In another recent study, *ex vivo* mechanical testing of brain tumor tissue confirmed its relative softness (Pogoda *et al.*, 2014). These findings are consistent with the results for implanted DBT tumors in our mouse model. Although our untreated group of mice only survived until POD13, the G′ value of the tumor ROI decreased over time in all but one mouse (Figure 4c). A similar pattern was observed in the radiation-treated group, in which the mean G′ values of the tumor ROIs (Figure 4a) were lower than those of the mirror ROIs, at all POD.

Currently, the efficacy of brain-tumor treatment is assessed by measuring changes in tumor size (James *et al.*, 1999; Macdonald *et al.*, 1990) using standard anatomic imaging modalities, such as CT (Leunens *et al.*, 1993; Lerch *et al.*, 1979; Constine *et al.*, 1988; Kortmann *et al.*, 1994) or MRI (Jost *et al.*, 2007; Shukla *et al.*, 2005; Ellingson *et al.*, 2015). However, changes in tumor size do not necessarily reflect changes in the internal properties of the tumors after radiation treatment. Average diffusion coefficient (ADC) values and fractional anisotropy (FA) values, derived from diffusion-weighted imaging, can serve as biomarkers of treatment response (Chenevert and Ross, 2009; Thoeny and Ross, 2010). The

ADC value has also been used to make pretreatment prediction of radiotherapy responses (Mardor et al., 2004), while other ADC-based metrics have been proposed for assessment of radiation response (Farjam et al., 2014). FA values were used as a biomarker of radiation injury (Chapman et al., 2012; Nagesh et al., 2008), though these studies did not include the longitudinal effects of radiation treatment. This study of the mechanical properties of tumors serves to establish MRE as another potential biomarker of tumor development and response to radiation therapy. The tumor properties probed by MRE are complementary to those measured by diffusion-weighted MRI. We anticipate incorporating both MRE and DWI into future studies, as we pursue our goal of developing a robust, reliable measure of early response to therapy.

This study presents results of the first longitudinal study of MRE-derived brain-tumor mechanical properties following radiation treatment. The decreasing shear modulus over time of both irradiated and non-irradiated tumor was significantly different from non-irradiated, contralateral tissue, a finding that indicates that DBT tumor tissue is significantly softer than contralateral (control) tissue. The mechanical properties of the tumor do not change significantly in response to radiation therapy. Thus, while MRE may have potential as a marker of therapeutic tumor response, the shear modulus of soft DBT-cell tumors, as measured by MRE in the mouse, is unaffected by radiation. The estimated G' values of the non-radiated ROIs at 1800 Hz were somewhat higher than reported previously (Clayton *et al.*, 2011a). The implanted tumor can alter the physiological environment of the brain, thus changing its mechanical properties compared with healthy tissue. The TLS inversion technique used, together with a different fitting window and filter, may also contribute to the observed differences in G' values. As in the study by Jost, et al. (2007), we observed a volume growth of tumor ROIs for later PODs. However, additional experiments are needed to determine whether this change in tumor volume is correlated with changes in tumor mechanical properties.

The study has several important limitations. The contours of the tumor ROI were drawn manually around hypointense ROIs in anatomical MR images, and, thus, may not precisely define the tumor (though the MRE results do not depend critically on these ROI borders). Although both G' and G'' values were reported, we focused primarily on G' values. While G' values were calculated on a voxel-by-voxel basis, all of our statistical tests were formulated based upon average G' values calculated for individual tumor ROIs, and, thus, do not reflect potential tumor heterogeneity. Although we report statistical significance for several of our results, the number of animals in this study was limited. By treating the contralateral side as control brain, we have ignored any effects that tumor implantation may have on the contralateral hemisphere. Planned future studies will test alternate tumor cell lines, incorporate more closely spaced time points, and include ex vivo mechanical testing of the tumor and surrounding brain tissue to examine tumor tissue in greater detail, and to provide additional support for our in vivo findings.

In summary, we have characterized the mechanical properties of mouse DBT-cell brain tumors using MRE and used tumor stiffness (G') as a biomarker for evaluating radiation treatment. The tumor region was softer than the healthy contralateral region and became softer over time, with or without radiation treatment. Radiation had a clear therapeutic

benefit, as indicated by increased survival of treated mice, but did not change the measured mechanical properties of the tissue at POD13 relative to non-irradiated tumor.

Acknowledgments

Grant 61503267 (YF) from Natural Science Foundation of China; BK20140356 (YF) from Jiangsu province; K511701515 (YF) from SRF for ROCS, SEM; NCI/NIH grant R01 CA155365 (JRG); Alvin J. Siteman Cancer Center (P30 CA091842), NSF grant CMMI-1332433 (PVB); and funding from the Mallinckrodt Institute of Radiology, Washington University in St. Louis, are acknowledged.

References

Atay SM, Kroenke CD, Sabet A, Bayly PV. Measurement of the dynamic shear modulus of mouse brain tissue in vivo by magnetic resonance elastography. J Biomech Eng. 2008; 130:021013. [PubMed: 18412500]

Barton MB, Harris R, Fletcher SW. Does this patient have breast cancer?: The screening clinical breast examination: should it be done? how? JAMA. 1999; 282:1270–80. [PubMed: 10517431]

Basu S, Alavi A. Molecular imaging (PET) of brain tumors. Neuroimaging clinics of North America. 2009; 19:625–46. [PubMed: 19959009]

Bolcaen J, Descamps B, Deblaere K, Boterberg T, De Vos Pharm F, Kalala JP, Van den Broecke C, Decrock E, Leybaert L, Vanhove C, Goethals I. (18)F-fluoromethylcholine (FCho), (18)F-fluoroethyltyrosine (FET), and (18)F-fluorodeoxyglucose (FDG) for the discrimination between high-grade glioma and radiation necrosis in rats: a PET study. Nuclear medicine and biology. 2015; 42:38–45. [PubMed: 25218024]

Chapman CH, Nagesh V, Sundgren PC, Buchtel H, Chenevert TL, Junck L, Lawrence TS, Tsien CI, Cao Y. Diffusion tensor imaging of normal-appearing white matter as biomarker for radiation-induced late delayed cognitive decline. International journal of radiation oncology, biology, physics. 2012; 82:2033–40.

Chenevert TL, Ross BD. Diffusion imaging for therapy response assessment of brain tumor. Neuroimaging clinics of North America. 2009; 19:559–71. [PubMed: 19959005]

Clayton EH, Garbow JR, Bayly PV. Frequency-dependent viscoelastic parameters of mouse brain tissue estimated by MR elastography. Physics in medicine and biology. 2011a; 56:2391. [PubMed: 21427486]

Clayton EH, Garbow JR, Bayly PV. Frequency-dependent viscoelastic parameters of mouse brain tissue estimated by MR elastography. Phys Med Biol. 2011b; 56:2391–406. [PubMed: 21427486]

Clayton EH, Genin GM, Bayly PV. Transmission, attenuation and reflection of shear waves in the human brain. Journal of the Royal Society Interface / the Royal Society. 2012; 9:2899–910.

Constine LS, Konski A, Ekholm S, McDonald S, Rubin P. Adverse effects of brain irradiation correlated with MR and CT imaging. International Journal of Radiation Oncology, Biology, Physics. 1988; 15:319–30.

Dunet V, Pomoni A, Hottinger A, Nicod-Lalonde M, Prior JO. Performance of 18F-FET versus 18F-FDG-PET for the diagnosis and grading of brain tumors: systematic review and meta-analysis. Neuro Oncol. 2015

Ellingson BM, Bendszus M, Boxerman J, Barboriak D, Erickson BJ, Smits M, Nelson SJ, Gerstner E, Alexander B, Goldmacher G, Wick W, Vogelbaum M, Weller M, Galanis E, Kalpathy-Cramer J, Shankar L, Jacobs P, Pope WB, Yang D, Chung C, Knopp MV, Cha S, van den Bent MJ, Chang S, Al Yung WK, Cloughesy TF, Wen PY, Gilbert MR. Consensus recommendations for a standardized Brain Tumor Imaging Protocol in clinical trials. Neuro-Oncology. 2015; 17:1188–98. [PubMed: 26250565]

Farjam R, Tsien CI, Feng FY, Gomez-Hassan D, Hayman JA, Lawrence TS, Cao Y. Investigation of the diffusion abnormality index as a new imaging biomarker for early assessment of brain tumor response to radiation therapy. Neuro Oncol. 2014; 16:131–9. [PubMed: 24327584]

Feng Y, Bayly P, Huang J, Robinson C, Du D, Mutic S, Shimony J, Leuthardt E, Okamoto R, Hu Y. A Simulation Study to Investigate the Potential of Using Magnetic Resonance Elastography (MRE) to Differentiate Recurrent Tumor and Radiation Necrosis. Medical physics. 2013a; 40:1.

Feng Y, Clayton EH, Chang Y, Okamoto RJ, Bayly PV. Viscoelastic properties of the ferret brain measured in vivo at multiple frequencies by magnetic resonance elastography. J Biomech. 2013b; 46:863–70. [PubMed: 23352648]

Garbow JR, McIntosh C, Conradi MS. Actively Decoupled Transmit-Receive Coil-Pair for Mouse Brain MRI Concepts in magnetic resonance. Part B, Magnetic resonance engineering. 2008; 33B: 252–9. [PubMed: 26207105]

Hakyemez B, Erdogan C, Ercan I, Ergin N, Uysal S, Atahan S. High-grade and low-grade gliomas: differentiation by using perfusion MR imaging. Clinical radiology. 2005; 60:493–502. [PubMed: 15767107]

Hatt A, Cheng S, Tan K, Sinkus R, Bilston LE. MR Elastography Can Be Used to Measure Brain Stiffness Changes as a Result of Altered Cranial Venous Drainage During Jugular Compression. Am J Neuroradiol. 2015; 36:1971–7. [PubMed: 26045579]

Horska A, Barker PB. Imaging of brain tumors: MR spectroscopy and metabolic imaging. Neuroimaging clinics of North America. 2010; 20:293–310. [PubMed: 20708548]

Huwart L, Peeters F, Sinkus R, Annet L, Salameh N, ter Beek LC, Horsmans Y, Van Beers BE. Liver fibrosis: non-invasive assessment with MR elastography. NMR Biomed. 2006; 19:173–9. [PubMed: 16521091]

James K, Eisenhauer E, Christian M, Terenziani M, Vena D, Muldal A, Therasse P. Measuring response in solid tumors: unidimensional versus bidimensional measurement. Journal of the National Cancer Institute. 1999; 91:523–8. [PubMed: 10088622]

John BW, Adam JP, Matthew DM, Irina MP, Jessica GS, Clifford JE, Lollis SS, Keith DP. Brain mechanical property measurement using MRE with intrinsic activation. Physics in medicine and biology. 2012; 57:7275. [PubMed: 23079508]

Johnson CL, McGarry MDJ, Gharibans AA, Weaver JB, Paulsen KD, Wang H, Olivero WC, Sutton BP, Georgiadis JG. Local mechanical properties of white matter structures in the human brain. NeuroImage. 2013; 79:145–52. [PubMed: 23644001]

Jost SC, Wanebo JE, Song SK, Chicoine MR, Rich KM, Woolsey TA, Lewis JS, Mach RH, Xu J, Garbow JR. In Vivo Imaging in A Murine Model of Glioblastoma. Neurosurgery. 2007; 60:360–71. 10.1227/01.NEU.0000249264.80579.37. [PubMed: 17290188]

Juhasz C, Dwivedi S, Kamson DO, Michelhaugh SK, Mittal S. Comparison of amino acid positron emission tomographic radiotracers for molecular imaging of primary and metastatic brain tumors. Molecular imaging. 2014; 13

Kortmann RD, Hess CF, Jany R, Bamberg M. Repeated CT examinations in limited volume irradiation of brain tumors: quantitative analysis of individualized (CT-based) treatment plans. Radiotherapy and Oncology. 1994; 30:171–4. [PubMed: 8184117]

Krouskop TA, Wheeler TM, Kallel F, Garra BS, Hall T. Elastic moduli of breast and prostate tissues under compression. Ultrasonic imaging. 1998; 20:260–74. [PubMed: 10197347]

Kumar M, Arlauckas SP, Saksena S, Verma G, Ittyerah R, Pickup S, Popov AV, Delikatny EJ, Poptani H. Magnetic resonance spectroscopy for detection of choline kinase inhibition in the treatment of brain tumors. Molecular cancer therapeutics. 2015; 14:899–908. [PubMed: 25657334]

Law M, Young RJ, Babb JS, Peccerelli N, Chheang S, Gruber ML, Miller DC, Golfinos JG, Zagzag D, Johnson G. Gliomas: predicting time to progression or survival with cerebral blood volume measurements at dynamic susceptibility-weighted contrast-enhanced perfusion MR imaging. Radiology. 2008; 247:490–8. [PubMed: 18349315]

Lerch IA, Carella RJ, Chiu-Tsao ST, Newall J. Assessment of the irradiated brain by quantitative computerized tomography scan analysis—I: Sampling methods and concepts. International J ournal of Radiation Oncology, Biology, Physics. 1979; 5:2121–6.

Leunens G, Menten J, Weltens C, Verstraete J, van der Schueren E. Quality assessment of medical decision making in radiation oncology: variability in target volume delineation for brain tumours. Radiotherapy and Oncology. 1993; 29:169–75. [PubMed: 8310142]

Leung D, Han X, Mikkelsen T, Nabors LB. Role of MRI in primary brain tumor evaluation. Journal of the National Comprehensive Cancer Network : JNCCN. 2014; 12:1561–8. [PubMed: 25361803]

Li J, Jamin Y, Boult JKR, Cummings C, Waterton JC, Ulloa J, Sinkus R, Bamber JC, Robinson SP. Tumour biomechanical response to the vascular disrupting agent ZD6126 in vivo assessed by magnetic resonance elastography. Br J Cancer. 2014; 110:1727–32. [PubMed: 24569471]

Lupo JM, Nelson SJ. Advanced magnetic resonance imaging methods for planning and monitoring radiation therapy in patients with high-grade glioma. Semin Radiat Oncol. 2014; 24:248–58. [PubMed: 25219809]

Macdonald DR, Cascino TL, Schold SC Jr, Cairncross JG. Response criteria for phase II studies of supratentorial malignant glioma Journal of clinical oncology : official journal of the American. S ociety of Clinical Oncology. 1990; 8:1277–80.

Mardor Y, Roth Y, Ochershvilli A, Spiegelmann R, Tichler T, Daniels D, Maier SE, Nissim O, Ram Z, Baram J, Orenstein A, Pfeffer R. Pretreatment prediction of brain tumors' response to radiation therapy using high b-value diffusion-weighted MRI. Neoplasia. 2004; 6:136–42. [PubMed: 15140402]

McKnight AL, Kugel JL, Rossman PJ, Manduca A, Hartmann LC, Ehman RL. MR elastography of breast cancer: preliminary results. AJR American journal of roentgenology. 2002; 178:1411–7. [PubMed: 12034608]

Minamimoto R, Saginoya T, Kondo C, Tomura N, Ito K, Matsuo Y, Matsunaga S, Shuto T, Akabane A, Miyata Y, Sakai S, Kubota K. Differentiation of Brain Tumor Recurrence from Post-Radiotherapy Necrosis with 11C-Methionine PET: Visual Assessment versus Quantitative Assessment. PLoS One. 2015; 10:e0132515. [PubMed: 26167681]

Moffat BA, Chenevert TL, Meyer CR, McKeever PE, Hall DE, Hoff BA, Johnson TD, Rehemtulla A, Ross BD. The functional diffusion map: an imaging biomarker for the early prediction of cancer treatment outcome. Neoplasia. 2006; 8:259–67. [PubMed: 16756718]

Murphy MC, Huston J, Glaser KJ, Manduca A, Meyer FB, Lanzino G, Morris JM, Felmlee JP, Ehman RL. Preoperative assessment of meningioma stiffness using magnetic resonance elastography. Journal of neurosurgery. 2013; 118:643–8. [PubMed: 23082888]

Muthupillai R, Lomas DJ, Rossman PJ, Greenleaf JF, Manduca A, Ehman RL. Magnetic-Resonance Elastography by Direct Visualization of Propagating Acoustic Strain Waves. Science. 1995; 269:1854–7. [PubMed: 7569924]

Nagesh V, Tsien CI, Chenevert TL, Ross BD, Lawrence TS, Junick L, Cao Y. Radiation-induced changes in normal-appearing white matter in patients with cerebral tumors: A diffusion tensor imaging study. Int J Radiat Oncol Biol Phys. 2008; 70:1002–10. [PubMed: 18313524]

Okamoto RJ, Clayton EH, Bayly PV. Viscoelastic properties of soft gels: comparison of magnetic resonance elastography and dynamic shear testing in the shear wave regime. Phys Med Biol. 2011; 56:6379–400. [PubMed: 21908903]

Pepin KM, Chen J, Glaser KJ, Mariappan YK, Reuland B, Ziesmer S, Carter R, Ansell SM, Ehman RL, McGee KP. MR Elastography Derived Shear Stiffness-A New Imaging Biomarker for the Assessment of Early Tumor Response to Chemotherapy. Magnetic Resonance in Medicine. 2014; 71:1834–40. [PubMed: 23801372]

Pogoda K, Chin LK, Georges PC, Byfield FJ, Bucki R, Kim R, Weaver M, Wells RG, Marcinkiewicz C, Janmey PA. Compression stiffening of brain and its effect on mechanosensing by glioma cells. New J Phys. 2014; 16:15.

Reiss-Zimmermann M, Streitberger KJ, Sack I, Braun J, Arlt F, Fritzsch D, Hoffmann KT. High Resolution Imaging of Viscoelastic Properties of Intracranial Tumours by Multi-Frequency Magnetic Resonance Elastography. Clinical neuroradiology. 2014

Sack I, McGowan CK, Samani A, Luginbuhl C, Oakden W, Plewes DB. Observation of nonlinear shear wave propagation using magnetic resonance elastography. Magn Reson Med. 2004; 52:842–50. [PubMed: 15389935]

Sahebjavaher RS, Nir G, Honarvar M, Gagnon LO, Ischia J, Jones EC, Chang SD, Fazli L, Goldenberg SL, Rohling R, Kozlowski P, Sinkus R, Salcudean SE. MR elastography of prostate cancer: quantitative comparison with histopathology and repeatability of methods. NMR in biomedicine. 2015; 28:124–39. [PubMed: 25395244]

Schmainda KM. Diffusion-weighted MRI as a biomarker for treatment response in glioma. CNS oncology. 2012; 1:169–80. [PubMed: 23936625]

Shukla D, Huilgol NG, Trivedi N, Mekala C. T2 weighted MRI in assessment of volume changes during radiotherapy of high grade gliomas. Journal of cancer research and therapeutics. 2005; 1:235–8. [PubMed: 17998661]

Simon M, Guo J, Papazoglou S, Scholand-Engler H, Erdmann C, Melchert U, Bonsanto M, Braun J, Petersen D, Sack I, Wuerfel J. Non-invasive characterization of intracranial tumors by magnetic resonance elastography. New J Phys. 2013; 15:14.

Sinkus R. Elasticity of the Heart, Problems and Potentials. Curr Cardiovasc Imaging Rep. 2014; 7:1–9.

Sinkus R, Lorenzen J, Schrader D, Lorenzen M, Dargatz M, Holz D. High-resolution tensor MR elastography for breast tumour detection. Physics in Medicine and Biology. 2000; 45:1649. [PubMed: 10870716]

Sinkus R, Tanter M, Xydeas T, Catheline S, Bercoff J, Fink M. Viscoelastic shear properties of in vivo breast lesions measured by MR elastography. Magnetic Resonance Imaging. 2005; 23:159–65. [PubMed: 15833607]

Suchorska B, Tonn JC, Jansen NL. PET imaging for brain tumor diagnostics. Current opinion in neurology. 2014; 27:683–8. [PubMed: 25333605]

Thoeny HC, Ross BD. Predicting and monitoring cancer treatment response with diffusion-weighted MRI. Journal of magnetic resonance imaging : JMRI. 2010; 32:2–16. [PubMed: 20575076]

Tsien C, Cao Y, Chenevert T. Clinical applications for diffusion magnetic resonance imaging in radiotherapy. Semin Radiat Oncol. 2014; 24:218–26. [PubMed: 24931097]

Uslu L, Donig J, Link M, Rosenberg J, Quon A, Daldrup-Link HE. Value of 18F-FDG PET and PET/CT for evaluation of pediatric malignancies. Journal of nuclear medicine : official publication, Society of Nuclear Medicine. 2015; 56:274–86.

Venkatesh SK, Yin M, Glockner JF, Takahashi N, Araoz PA, Talwalkar JA, Ehman RL. MR Elastography of Liver Tumors: Preliminary Results. American Journal of Roentgenology. 2008; 190:1534–40. [PubMed: 18492904]

Wang Y, Ganger DR, Levitsky J, Sternick LA, McCarthy RJ, Chen ZE, Fasanati CW, Bolster B, Shah S, Zuehlsdorff S, Omary RA, Ehman RL, Miller FH. Assessment of chronic hepatitis and fibrosis: comparison of MR elastography and diffusion-weighted imaging. AJR Am J Roentgenol. 2011; 196:553–61. [PubMed: 21343496]

Xu L, Lin Y, Han JC, Xi ZN, Shen H, Gao PY. Magnetic resonance elastography of brain tumors: Preliminary results. Acta Radiol. 2007; 48:327–30. [PubMed: 17453505]

Yin M, Talwalkar JA, Glaser KJ, Manduca A, Grimm RC, Rossman PJ, Fidler JL, Ehman RL. Assessment of hepatic fibrosis with magnetic resonance elastography. Clinical gastroenterology and hepatology : the official clinical practice journal of the American Gastroenterological Association. 2007; 5:1207–13 e2. [PubMed: 17916548]

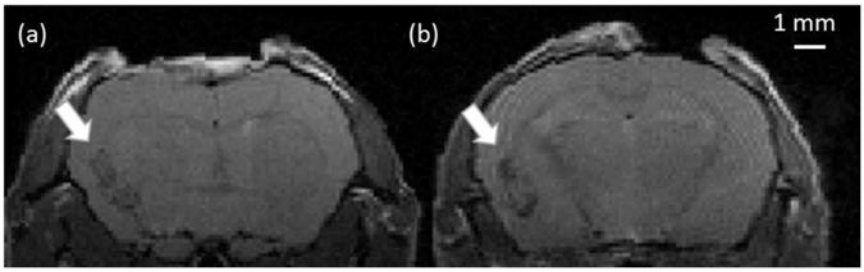

Figure 1.

Anatomical MR images of a mouse brain on POD8: (a) M07B, and (b) M05B. Tumors, which appear hypointense in the images, were implanted in the left hemisphere. The voxel size is $0.125 \times 0.125 \times 0.5\ mm^3$.

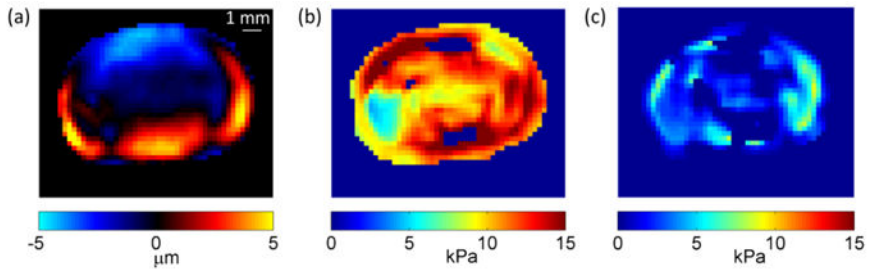

Figure 2.

(a) The imaginary component of the fundamental harmonic of the through-plane displacement field of a mouse brain (M10A) at 1800 Hz. Distribution of (b) G' and (c) G'' value of the same mouse brain for Nxy=2 and δ=0.1.

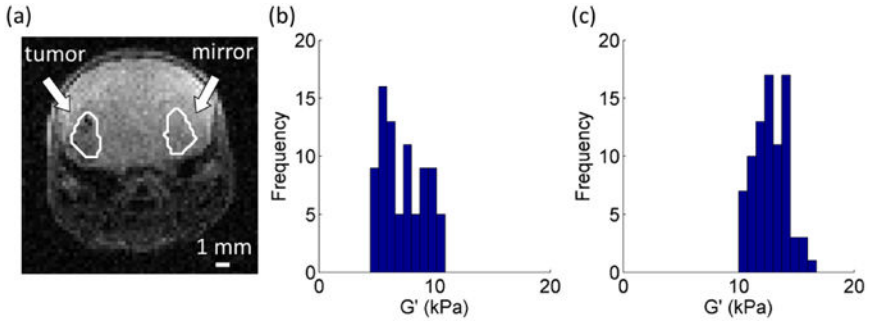

Figure 3.

(a) Manually delineated tumor and mirror ROIs. Histogram of the G′ values of the (b) tumor and (c) mirror ROIs from Figure 2a. The number of bins for each histogram was calculated as the square root of the total number of voxels for each delineated region. A total of 9 bins were used to group the 82 voxels in the contoured tumor and mirror regions.

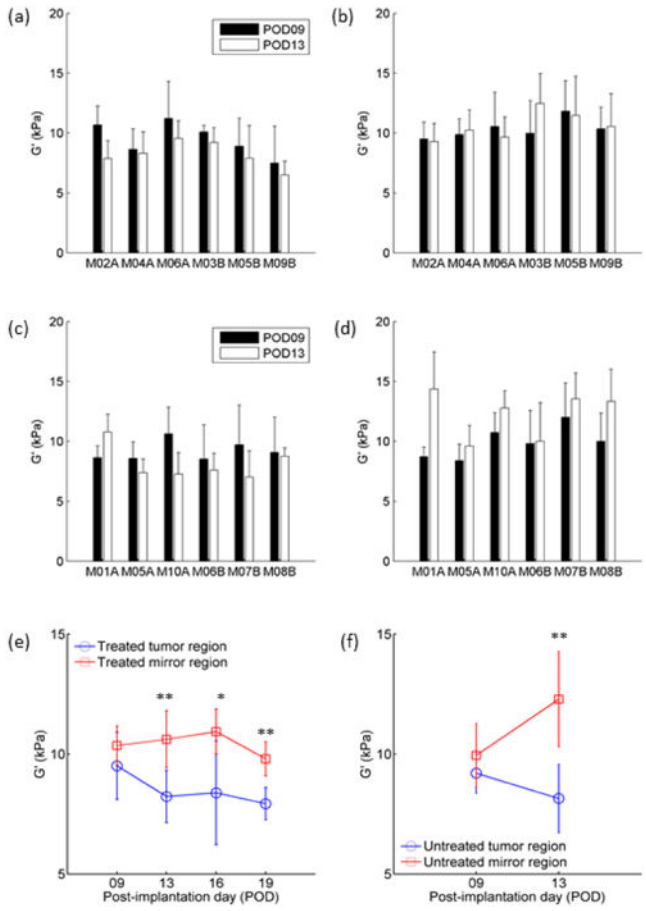

Figure 4.

Comparison of the G′ values of tumor and mirror ROIs at POD09 and POD13 before and after radiation treatment. (a-b) Treated group: G′ values at POD09 and POD13 for the (a) tumor ROI and (b) its contralateral mirrored ROI, in each animal; (c-d) Untreated group: G′ values at POD09 and POD13 for the (c) tumor ROI and (d) its contralateral mirrored ROI, in each animal. The markers and error bars represent the mean values and standard deviations estimated using all voxels in the corresponding ROI for all mice in (e) the treated group and (f) untreated group, shown vs. time after implantation. Note: vertical axis limits are set to 5 kPa – 15 kPa to illuminate differences between curves. A paired Student T-test was carried out to compared the G″ value of the tumor and mirror ROI groups at each POD. The “*” and “**” symbols indicate a significant difference of the G″ value between the tumor and mirror ROIs, with significance levels of 5% and 2%, respectively.

Table 1

Mean and standard deviation of the G″ values of the tumor and mirror ROI in both the treated and untreated group. Asterisks indicate a significant difference between the tumor and mirror ROIs†

	G″ (kPa) value of the treated group			G″ (kPa) value of the untreated group		
	Tumor ROI	**Mirror ROI**	**Significance level**	**Tumor ROI**	**Mirror ROI**	**Significance level**
POD09	3.48±1.59	3.06±1.77	-	2.78±2.19	4.53±3.35	-
POD13	3.06±1.01	3.30±1.86	-	2.72±0.89	4.30±1.20	*
POD16	2.60±0.79	3.91±0.98	**	-	-	-
POD19	2.77±0.60	3.76±0.91	-	-	-	-

†A paired student t-test was carried out to compared the G″ value of the tumor and mirror ROI groups at each POD.

The “*” and “**” symbols indicate a significant difference of the G″ value between the tumor and mirror ROIs, with significance levels of 5% and 2%, respectively.

Phys Med Biol. Author manuscript; available in PMC 2018 May 10.